Cell

Molecular Basis of RNA Polymerase III Transcription Repression by Maf1

Alessandro Vannini,[1,3] Rieke Ringel,[1,3] Anselm G. Kusser,[1,3] Otto Berninghausen,[1] George A. Kassavetis,[2] and Patrick Cramer[1,*]

[1]Gene Center and Department of Biochemistry, Center for Integrated Protein Science Munich (CIPSM), Ludwig-Maximilians-Universität München, Feodor-Lynen-Strasse 25, 81377 Munich, Germany

[2]Division of Biological Sciences, University of California, San Diego, 9500 Gilman Drive, La Jolla, CA 92093-0634, USA

[3]These authors contributed equally to this work

*Correspondence: cramer@genzentrum.lmu.de

DOI 10.1016/j.cell.2010.09.002

SUMMARY

RNA polymerase III (Pol III) transcribes short RNAs required for cell growth. Under stress conditions, the conserved protein Maf1 rapidly represses Pol III transcription. We report the crystal structure of Maf1 and cryo-electron microscopic structures of Pol III, an active Pol III-DNA-RNA complex, and a repressive Pol III-Maf1 complex. Binding of DNA and RNA causes ordering of the Pol III-specific subcomplex C82/34/31 that is required for transcription initiation. Maf1 binds the Pol III clamp and rearranges C82/34/31 at the rim of the active center cleft. This impairs recruitment of Pol III to a complex of promoter DNA with the initiation factors Brf1 and TBP and thus prevents closed complex formation. Maf1 does however not impair binding of a DNA-RNA scaffold and RNA synthesis. These results explain how Maf1 specifically represses transcription initiation from Pol III promoters and indicate that Maf1 also prevents reinitiation by binding Pol III during transcription elongation.

INTRODUCTION

The eukaryotic genome is transcribed by the multisubunit enzymes Pol I, II, and III, which catalyze DNA-dependent RNA synthesis. Pol III transcribes genes encoding short, untranslated RNAs, including transfer RNAs, 5S ribosomal RNA (rRNA), the spliceosomal U6 small nuclear RNA (snRNA), and the signal recognition particle 7SL RNA. Pol III genes are essential and involved in fundamental processes such as ribosome and protein biogenesis, RNA processing, and protein transport. Pol III transcription is coregulated with Pol I activity, accounting together for up to 80% of nuclear gene transcription in growing cells (Paule and White, 2000; Grummt, 2003; Willis et al., 2004). Pol III activity is a critical determinant of cell growth.

Pol III is the most complex of the nuclear RNA polymerases. It has a total molecular weight of around 700 kDa and comprises 17 subunits (Schramm and Hernandez, 2002). Five of its subunits, Rpb5, 6, 8, 10, and 12, are common to Pol I, II, and III. Subunits AC40 and AC19 are common to Pol I and III and are homologous to Pol II subunits Rpb3 and Rpb11, respectively. The two largest Pol III subunits C160 and C128 are homologous to Pol II subunits Rpb1 and Rpb2, respectively, and form the active center of the enzyme. Subunits C17 and C25 form a subcomplex with homology to the Pol II subcomplex Rpb4/7 (Ferri et al., 2000; Jasiak et al., 2006; Sadhale and Woychik, 1994), whereas subunit C11 shares homology with Pol II subunit Rpb9. The Pol III-specific subunits C82, C53, C37, C34, and C31 form two subcomplexes. The C53/37 subcomplex shows weak homology to the Pol II initiation factor TFIIF and is involved in promoter opening, elongation, termination, and reinitiation (Cramer et al., 2008; Carter and Drouin, 2009; Kassavetis et al., 2010; Landrieux et al., 2006), whereas the C82/34/31 subcomplex is involved in promoter recognition and initiation. C34 interacts with TFIIIB, which recruits Pol III to promoters (Thuillier et al., 1995; Wang and Roeder, 1997; Werner et al., 1993) and is involved in open complex formation (Brun et al., 1997). To date, structural information on Pol III is limited to a cryo-electron microscopic (cryo-EM) map that revealed the approximate location of the two Pol III-specific subcomplexes (Fernández-Tornero et al., 2007), a homology model for the 10-subunit core enzyme, and the crystal structure of C25/17 (Jasiak et al., 2006).

Rapid repression of Pol III transcription ensures cell survival during stress (Warner, 1999). Pol III repression is mediated by Maf1, a protein that is conserved from yeast to human (Pluta et al., 2001; Upadhya et al., 2002). Maf1 represses Pol III in response to DNA damage, oxidative stress, growth to stationary phase, treatment with rapamycin or chlorpromazine, and blocking of the secretory pathway (Upadhya et al., 2002; Willis et al., 2004). In growing yeast, Maf1 is phosphorylated and localized in the cytoplasm. Stress conditions lead to Maf1 dephosphorylation and nuclear import (Oficjalska-Pham et al., 2006; Roberts et al., 2006), which is directed by two nuclear localization signal (NLS) sequences (Lee et al., 2009; Moir et al., 2006). In the nucleus, Maf1 binds Pol III to prevent its interaction with TFIIIB and promoters (Desai et al., 2005; Moir et al., 2006; Roberts et al., 2006). Maf1 also binds Brf1, a subunit of TFIIIB that resembles the Pol II initiation factor

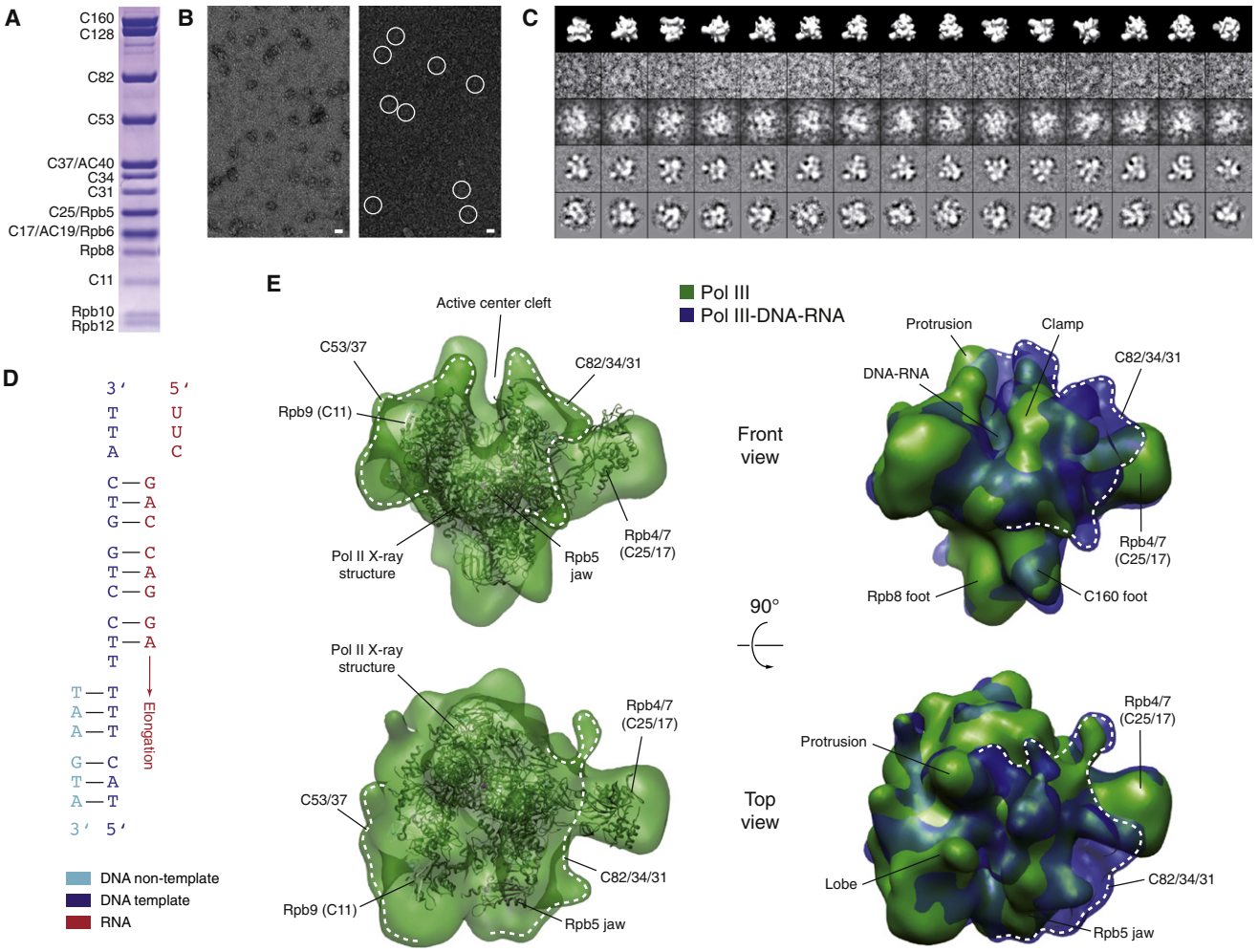

Figure 1. Cryo-EM Structures of Pol III and Pol III-DNA-RNA Complex

(A) SDS-PAGE of pure yeast Pol III. The identity of the 17 subunits was confirmed by mass spectrometry.

(B) EM micrographs of Pol III in negative stain (left) and vitrified ice (right). Scale bars represent 10 nm.

(C) Views of the Pol III reconstruction (first row) with corresponding raw single-particle images (second row), low pass-filtered single-particle images (third row), class averages (forth row), and reference-free averages (fifth row).

(D) DNA-RNA scaffold used in complex formation.

(E) Cryo-EM reconstruction of Pol III (green) and Pol III-DNA-RNA complex (blue). The Pol II X-ray structure (Armache et al., 2005) was fitted to the Pol III map and is shown as a ribbon model. White dashed lines indicate additional densities between the lobe and Rpb9 (C11), attributed to the C53/37 subcomplex, and between the clamp and Rpb5, attributed to the C82/34/31 subcomplex, that gets ordered in the DNA-RNA complex.

See also Figures S1 and S4 and Movie S1.

TFIIB (Desai et al., 2005). Maf1-mediated repression is associated with reduced Brf1 and Pol III occupancy at Pol III genes (Oficjalska-Pham et al., 2006; Roberts et al., 2006). Similar results have been obtained with human cells, establishing Maf1 as a conserved global repressor of Pol III transcription (Reina et al., 2006).

Here, we report cryo-EM structures of Pol III in its free form and in complex with a DNA-RNA scaffold, assign the locations of Pol III subunits, present the Maf1 crystal structure, and combine the resulting information with a cryo-EM structure of a Pol III-Maf1 complex. Together with functional studies, these results establish the mechanism for Pol III transcription repression by Maf1.

RESULTS AND DISCUSSION

Pol III EM Structure Reveals C82/34/31 Mobility

We established a protocol for large-scale purification of Pol III from the yeast *Saccharomyces cerevisiae* (Experimental Procedures). Pure Pol III samples comprised all 17 subunits (Figure 1A), were monodisperse, and appeared homogeneous in EM with negative stain (Figure 1B). We collected high-quality cryo-EM data after vitrification under native conditions. A reconstruction of Pol III from 20,480 single particles led to a map at 21 Å resolution (Figure 1E; Figure S1 available online; Experimental Procedures) that generally agrees with the previously published map (Fernández-Tornero et al., 2007).

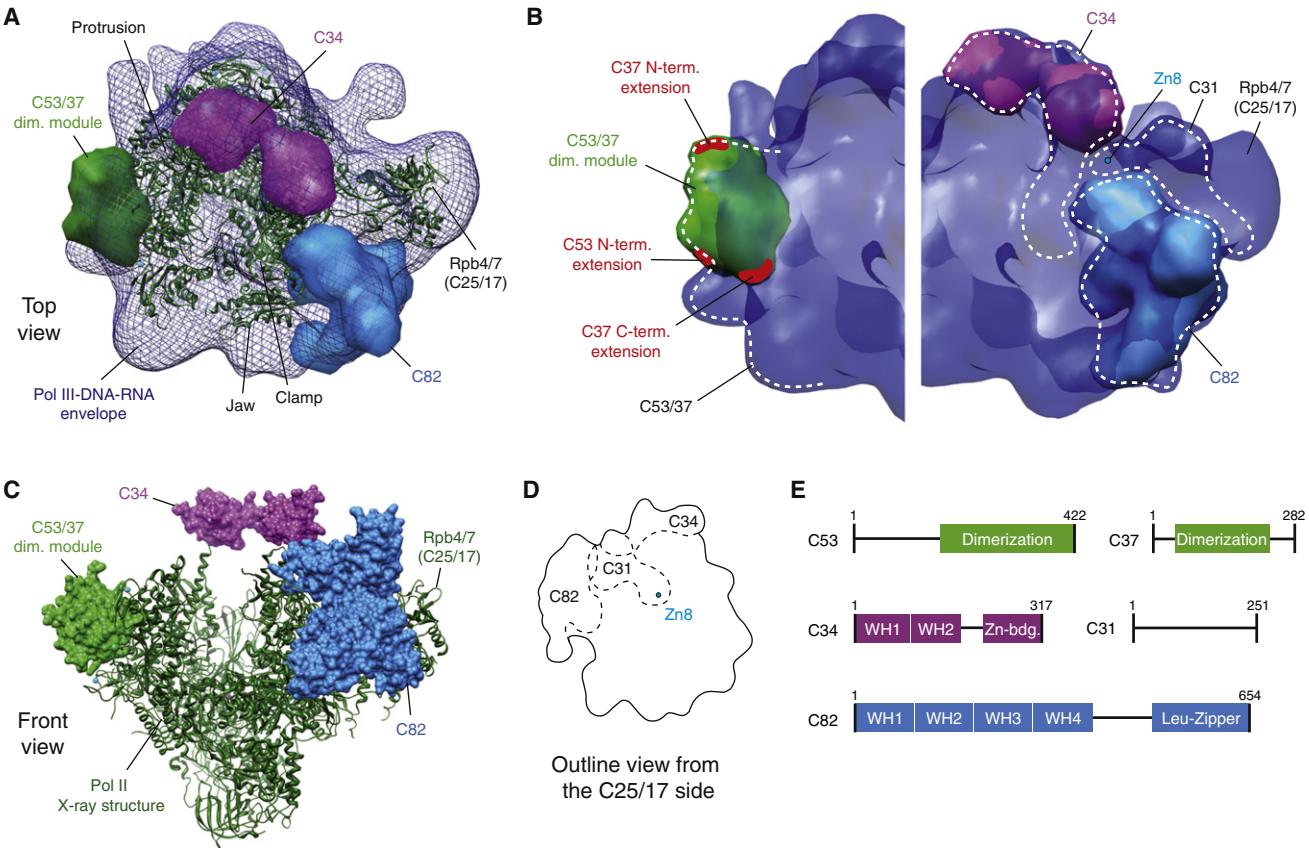

Figure 2. Subunit Architecture of Pol III

(A) Pol III-specific subunits were placed into the cryo-EM envelope of the Pol III-DNA-RNA complex. A homology model of the C53/37 dimerization domain (green) (Geiger et al., 2010), the human C82 homolog crystal structure (blue; S. Fribourg, personal communication), and the two C34 WH domain crystal structures (purple) are shown as molecular surfaces. Fitted structures are shown low-pass filtered to the same resolution than the EM map. The 12 subunit Pol II X-ray structure (Armache et al., 2005) is shown as a green ribbon.

(B) Close-up views of Pol III-specific subunits fitted into the cryo-EM envelope of the Pol III-DNA-RNA complex. Terminal extensions of the C53/37 dimerization module are highlighted in red.

(C) Location of Pol III-specific subunits on the Pol II structure. The view is related to the one in (A) by a 90° rotation around a horizontal axis.

(D) Location of subunits of the C82/34/31 subcomplex within Pol III.

(E) Domain organization of Pol III-specific subunits. Based on homology modeling (C53, C37), crystallography (C34), or HHPred and secondary structure prediction (C82).

See also Figures S2 and S4 and Movie S1.

The 12-subunit Pol II crystal structure (Armache et al., 2005) was unambiguously fitted to the EM map (Figure 1E). After that, two densities remained that could not be assigned to Pol III-specific insertions or residues lacking from the Pol II structure, one at the polymerase lobe and one on top of the clamp (Figure 1E). Densities at the lobe and clamp were attributed to subcomplexes C53/37 and C82/34/31, respectively (Fernández-Tornero et al., 2007). The density at the lobe was fitted with a homology model of the C53/37 dimerization module based on the structure of the related A49/34.5 module in Pol I (Geiger et al., 2010) (Figure 2). The location of C53/37 agrees with the previously reported association of C53/37 with C11 (Chédin et al., 1998) and with the location of the TFIIF dimerization domain on the Pol II lobe (Chen et al., 2010; Eichner et al., 2010). The additional density at the clamp accounts only for part of the 138 kDa subcomplex C82/34/31, indicating flexibility (Figure 1E).

Nucleic Acid Binding Restricts C82/34/31

To see how nucleic acid binding influences the Pol III structure, we determined the cryo-EM structure of a Pol III complex with a minimal DNA-RNA scaffold (Figure 1D; Experimental Procedures). This complex mimics an active elongation complex (Brueckner et al., 2007). A reconstruction at 19 Å resolution was obtained from 11,965 single particles (Figure 1E). The reconstruction revealed density for nucleic acids in the cleft, but also a structural ordering of the C82/34/31 subcomplex, giving rise to an extended density between the top of the clamp, the Rpb5 jaw, and C25/17 (Figures 1E and 2A; Figure S2).

A continuous density between the clamp and the jaw could be fitted with the crystal structure of the human C82 homolog (S. Fribourg, personal communication) (Figure 2). A prominent density remained, forming a suspension over the cleft from the clamp to the protrusion (Figures 1E and 2A–2C). This density

was assigned to subunit C34 since its two lobes fitted the structures of two winged helix (WH) domains in C34 (PDB codes 2dk5 and 2dk8), and since C34 crosslinks to promoter DNA around position −21 (Bartholomew et al., 1993), which is adjacent in the homologous Pol II promoter complex model (Kostrewa et al., 2009). The remaining globular density between the clamp and C25/17 (Figure 2; Figure S2) was assigned to C31 since this position explains the known interactions of C31 with subunits C160, C82, C34, and C17 (Chédin et al., 1998; Geiduschek and Kassavetis, 2001; Schramm and Hernandez, 2002), the requirement of the adjacent zinc site Zn8 in C160 for C82/34/31 binding (Werner et al., 1992), and association of C31 with Pol III after dissociation of the C82/34 heterodimer (Lorenzen et al., 2007). Thus, all Pol III subunits were assigned to EM densities consistent with known subunit interactions.

Globular Structure of Maf1

To elucidate Pol III repression by Maf1, we determined the Maf1 structure by X-ray crystallography (Experimental Procedures). Limited proteolysis of recombinant *S. cerevisiae* and human Maf1 revealed two flexible regions, a mobile insertion and an acidic C-terminal tail (Figure 3A). A human variant that lacked both mobile regions crystallized. The structure was solved by bromide phasing and refined to a free R factor of 21.2% at 1.55 Å resolution (Table 1). Maf1 forms a globular structure with a central five-stranded antiparallel β sheet that is flanked by one helix on one side and three helices on the other (Figure 3B). The Maf1 fold is frequently observed, but not in proteins involved in transcription (Holm and Park, 2000; Krissinel and Henrick, 2004). The structure shows that the previously defined conserved sequence boxes A, B, and C (Desai et al., 2005; Pluta et al., 2001; Reina et al., 2006) do not correspond to structural modules or defined surface patches (Figure 3C). Thus, functional data for Maf1 deletion variants must be re-evaluated in light of the structure. The Maf1 structure is conserved among eukaryotes, since hydrophobic core residues are conserved from yeast to human (Figure 3A).

Regulated Maf1 Localization

The Maf1 crystal structure reveals that the two NLS sequences (yeast residues 205–208 and 328–332; Moir et al., 2006) are surface accessible (Figure 3B). The C-terminal NLS (Ct-NLS) is located between strands β4 and β5, and the N-terminal NLS (Nt-NLS) is part of the directly adjacent mobile region (Figure 3B). The adjacent location suggests that phosphorylation of the mobile insertion regulates nuclear localization by masking the NLS sequences (Lee et al., 2009; Moir et al., 2006). This mechanism is apparently conserved from yeast to human, although the phosphorylation sites within the mobile insertion differ (Dephoure et al., 2008; Lee et al., 2009; Moir et al., 2006; Shor et al., 2010). The Ct-NLS and adjacent residues form the only positively charged region on Maf1 (Figure 3F). Several point mutants that lead to defects in phosphorylation, growth on glycerol at 37°C, or Pol III repression (Moir et al., 2006; Roberts et al., 2006) are exposed around the mobile insertion (Figure 3E, residues labeled in red and pink).

Maf1 Rearranges C82/34/31

To investigate how Maf1 binds yeast Pol III, we prepared full-length recombinant yeast Maf1 and a variant that lacked both mobile regions (residues 36–224 and 346–395) and corresponded to the crystallized human protein. Both variants formed a complex with Pol III that could be purified by size-exclusion chromatography (Figure 3D, lanes 3 and 4). Maf1 binding was specific, as human Maf1 did not bind yeast Pol III (data not shown). Thus, the two mobile regions are not required for Pol III binding, and the human Maf1 crystal structure is relevant for understanding the Pol III-Maf1 interaction in the yeast system. We collected cryo-EM data of the pure Pol III-Maf1 complex and used 16,974 particles to obtain a reconstruction at 18.5 Å resolution (Figure 4; Figure S3; Experimental Procedures). The structure revealed a continuous density for C82/34/31, similar to the density in the Pol III-DNA-RNA complex (Figure 4C; Figure S5).

Maf1 was assigned to a new density on top of the clamp with the help of difference maps (Figure 4; Figure S3). The Maf1 X-ray structure fitted this density well (Figures 4A and 4C; Figure S3). To provide additional support for the Maf1 location, we labeled the C-terminal hexahistidine tags on Maf1 and the Pol III subunit C128 with Ni-NTA-Nanogold and located the labels by 2D cryo-EM image analysis (Experimental Procedures). The locations of the labels were consistent with Maf1 binding on top of the clamp domain (Figure 4B). This location also agreed with published biochemical and genetic interactions of Maf1 with the N-terminal region of C160, which forms most of the clamp (Boguta et al., 1997; Oficjalska-Pham et al., 2006; Reina et al., 2006) (Figure 4D). Further consistent with this location, C160, C82, and C34 are the key interacting partners of Maf1 in the yeast interactome (Gavin et al., 2006).

Maf1 partially overlapped with the assigned locations of the second WH domain in C34 and with C82 and C31 in the Pol III-DNA-RNA complex (Figures 4C and 4E). Consistently, the C82/34/31 density in the Pol III-Maf1 complex differed from that in the Pol III-DNA-RNA complex. Most of the density assigned to the C34 WH domains in the Pol III-DNA-RNA complex was absent in the Pol III-Maf1 complex, indicating a Maf1-dependent displacement of these domains (Figure 4F; Figure S3). The densities assigned to C31 and C82 apparently shifted toward the Rpb5 jaw (Figures 4C and 4F; Figure S3). The differences in the EM structures are visualized in a side-by-side comparison and a movie (Figure S4; Movie S1).

Maf1 Impairs Closed Promoter Complex Formation

To analyze how the structural changes induced by Maf1 could repress Pol III transcription, we modeled the Pol III-Brf1-TBP closed promoter complex. Brf1 resembles the Pol II initiation factor TFIIB in its N-terminal region but contains a specific C-terminal extension that binds TBP (Figure S5) (Khoo et al., 1994). We combined the Pol II-TFIIB-TBP closed promoter complex model (Kostrewa et al., 2009) with the structure of TBP bound to the Brf1 C-terminal residues 437–507 (Juo et al., 2003). Comparison of the resulting model with the EM densities revealed that C34 was well positioned for interacting with the Brf1 N- and C-terminal regions (Figure 5A), consistent with published data (Khoo et al., 1994, Andrau et al., 1999; Brun et al., 1997; Kassavetis et al., 2003). In the Pol III-Maf1 complex,

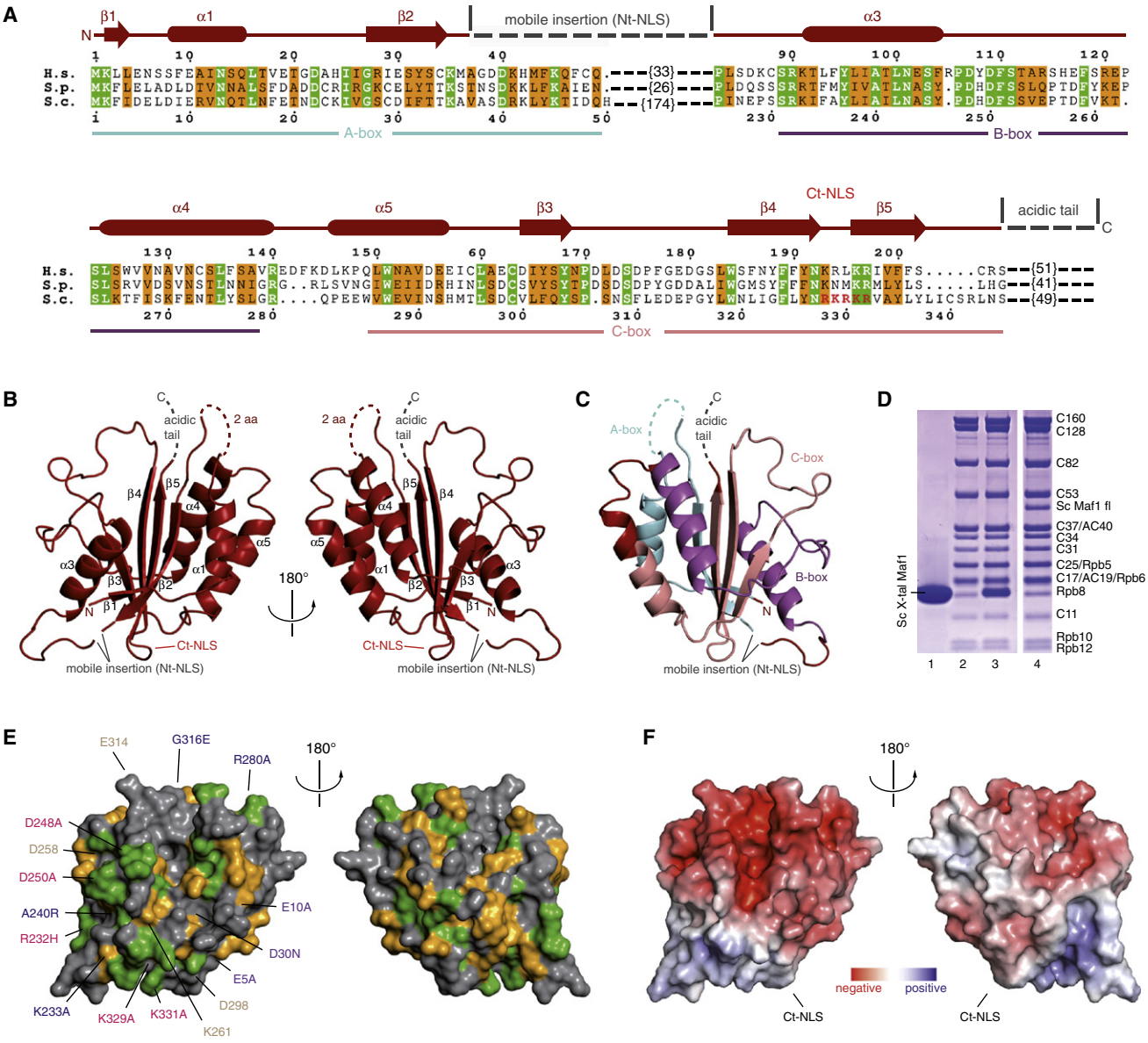

Figure 3. Maf1 Crystal Structure

(A) Amino acid sequence alignment of Maf1 from *Homo sapiens* (H.s.), *Schizosaccharomyces pombe* (S.p.), and *Saccharomyces cerevisiae* (S.c.). Secondary structure elements are indicated (cylinders, α helices; arrows, β strands). Identical and conserved residues are highlighted in green and orange, respectively. The mobile insertion (human residues 36–82, yeast residues 36–224) includes proteolytic cleavage sites (this work), phosphorylation sites (Dephoure et al., 2008; Lee et al., 2009; Moir et al., 2006), and the N-terminal NLS (Nt-NLS). The C-terminal NLS (Ct-NLS) is indicated. Dashed lines indicate regions absent from the crystal structure. The crystallized protein is a human Maf1 variant comprising residues 1–35 and 83–205.

(B) Two views of a ribbon model of the Maf1 crystal structure. Secondary structure elements are labeled according to (A).

(C) Maf1 ribbon model with the conserved boxes A, B, and C highlighted in blue, purple, and rose, respectively.

(D) Purification of Pol III-Maf1 complexes. Two hundred microrams of Pol III and a 5-fold molar excess of full-length yeast Maf1 or a variant comprising residues 1–35 and 225–345 (lane 1) were incubated for 20 min at 20°C, subjected to gel filtration, and analyzed by SDS-PAGE. Lanes 2, 3, and 4 show Pol III, the Pol III complex with the Maf1 variant, and the Pol III complex with full-length Maf1, respectively.

(E) Surface conservation of Maf1. Identical and conserved residues are highlighted in green and yellow, respectively. Mutations at residues labeled in red, pink, and wheat show severe, mild, or no phenotypes, respectively (Dephoure et al., 2008; Moir et al., 2006; Roberts et al., 2006).

(F) Surface charge distribution of Maf1. Red, blue, and white areas indicate negative, positive, and neutral charge, respectively.

C34 adopts a different position that is apparently incompatible with Brf1 interaction, suggesting that Maf1 impairs Pol III recruitment to Brf1-containing promoters (Figures 5A and 5B).

To test this model, we investigated by size-exclusion chromatography whether the Pol III-Maf1 complex can bind to a preassembled functional Brf1-TBP-DNA promoter complex

Table 1. Maf1 X-Ray Diffraction and Refinement Statistics

Data Set	NaBr Soak			Native
Data Collection				
Space group	P $2_12_12_1$			P $2_12_12_1$
Unit cell axis: *a, b, c* (Å)	48.1, 48.3, 80.5			48.4, 48.8, 79.3
	Peak	Remote	Inflection	
Wavelength (nm)	0.9196	0.9211	0.9200	0.91870
Resolution (Å)[a]	26.83–1.9	26.83–1.9	26.83–1.9	25.974–1.55
R_{merge} (%)[a]	7.7 (50.7)	6.0 (39.2)	7.0 (51.3)	5.2 (58.9)
I/σ (I)[a]	22.0 (2.5)	22.7 (3.0)	22.0 (2.4)	22.3 (1.2)
Completeness (%)[a]	99.0 (99.5)	98.8 (99.4)	98.9 (99.5)	94.3 (87.4)
Redundancy[a]	3.9 (4.0)	3.8 (3.9)	3.8 (4.0)	3.0 (1.9)
Refinement				
Resolution (Å)				1.55–25.97
Number of reflections				26,183
R_{work} (%)				18.81
R_{free} (%)				21.15
Number of atoms				
Protein				1313
Water				142
B factors (Å^2)				
Protein				33.64
Water				43.95
Rmsd from ideal				
Bond lengths (Å)				0.006
Bond angles (°)				0.959

$R_{merge} = \Sigma\ |I - < I >|/\Sigma\ |$ where I is the integrated intensity of a given reflection.

$R = \Sigma\ ||F_{obs}| - |F_{calc}||/\Sigma\ |F_{obs}|$. R_{free} was calculated with 5% of data excluded from refinement.

[a] The highest-resolution shell is shown in parentheses.

(Kassavetis et al., 2005). We used U6 snRNA promoter DNA from position −40 to +20 relative to the transcription start site +1 (Figure 6A, closed scaffold). Whereas free Pol III stably bound the Brf1-TBP-DNA complex, the Pol III-Maf1 complex did not, even when a 5-fold molar excess was used (Figure 6B, lanes 3, 5). When we repeated the experiment with a mismatched bubble region at positions –11 to +2 (Figure 6A, bubble scaffold), the same result was obtained (Figure 6E, lanes 6, 7). Further, preassembled Pol III-Brf1-TBP-DNA complex did not bind Maf1, even when a 5-fold molar excess was used (Figure 6B, lane 4). Thus, the interactions of Pol III with Maf1 and a Brf1-TBP-DNA complex are mutually exclusive, showing that Maf1 impairs formation of a closed promoter complex. This is consistent with evidence that Maf1 prevents Pol III promoter interaction (Desai et al., 2005; Moir et al., 2006; Roberts et al., 2006).

Maf1 Does Not Inhibit Pol III Activity

The above model predicts that Maf1 inhibits binding of promoter DNA over the active center cleft, but not in the cleft. To test this, we compared pure Pol III and Pol III-Maf1 complexes in an initiation factor-independent transcription assay using a 3′-tailed DNA template and a priming RNA dinucleotide (Bardeleben et al., 1994). Consistent with the model, both complexes were equally active in RNA synthesis, and an excess of Maf1 or DNA did not change activity (Figure 6C). We also performed RNA extension assays using a minimal DNA-RNA scaffold (Damsma and Cramer, 2009). The presence of Maf1 neither prevented scaffold binding nor elongation to the end of the template, and this was independent of the order of factor addition (Figure 6D).

To rule out that nucleic acids displace Maf1 from Pol III or prevent its binding, we tested by size-exclusion chromatography whether Pol III binds Maf1 and nucleic acids simultaneously. Pol III-Maf1 complexes with tailed template or bubble scaffold could be purified, independent of the order of addition (Figure 6E). Thus, Maf1 prevents neither nucleic acid binding in the active center nor RNA synthesis. The observation that Pol III can simultaneously bind Maf1 and nucleic acids suggests that the increased Maf1 occupancy at Pol III genes under repressive conditions (Geiduschek and Kassavetis, 2006; Oficjalska-Pham et al., 2006; Roberts et al., 2006) is due to Maf1 binding to elongation complexes. Pol III in such Maf1-containing elongation complexes would be unable to reinitiate, explaining the observation that Maf1 represses multiple-round transcription by Pol III (Cabart et al., 2008).

Conclusions

Our results converge with published data on the mechanism of Pol III-specific transcription repression by Maf1. Cellular stress leads to dephosphorylation of a mobile surface region in Maf1 that unmasks adjacent NLS sequences, leading to nuclear import of Maf1. In the nucleus, Maf1 binds free Pol III at its clamp domain and rearranges the C82/34/31 subcomplex. This impairs Pol III binding to a TBP-Brf1-promoter complex and specifically abolishes initiation from Pol III promoters, which require Brf1. Maf1 also binds Pol III that is engaged in transcription elongation, leaving activity intact but preventing reinitiation. Since Pol III genes are short and elongation is fast, this leads to rapid shutdown of all Pol III transcription.

EXPERIMENTAL PROCEDURES

Pol III Preparation

The *Saccharomyces cerevisiae* strain NZ16 (Lannutti et al., 1996), carrying the gene for an N-terminally His_6-$FLAG_4$-RET1-tagged C128 subunit on the parent plasmid pYE(CEN3)30 was grown to OD_{600} = 6–7 at 30°C in YPD media in a 200 L fermenter (Infors ABEC). Cells were lysed by bead beating in ice-cooled buffer A [200 mM Tris-HCl (pH 8.0), 500 mM $(NH_4)_2SO_4$, 10 mM $MgCl_2$, 10% glycerol, 10 mM β-mercaptoethanol, 1 mM PMSF, 1 mM benzamidine, 200 mM pepstatin, 60 mM leupeptin]. Subsequent steps were performed at 4°C. Glass beads were separated by filtration, and the lysate was cleared by centrifugation (60 min, 8000 g, Sorvall SLA-1500). A whole-cell extract was obtained after centrifugation at 125,000 g for 90 min (Beckman Ti45) by separation of the clear upper-middle phase from the turbid lower phase. The supernatant was processed by step-wise ammonium sulfate precipitation. Thirty-five percent $(NH_4)_2SO_4$ was added, and the sample was stirred for 30 min and cleared by centrifugation (60 min, 8000 g, Sorvall SLA-1500). The supernatant was precipitated over night after addition of 70% $(NH_4)_2SO_4$. The pellet was recovered by centrifugation (60 min, 8000 g, Sorvall SLA-1500) and resuspended in 3 liters of buffer B (40 mM HEPES [pH 7.8], 5 mM $MgCl_2$, 10% glycerol, 1 mM EDTA, 10 mM β-mercaptoethanol,

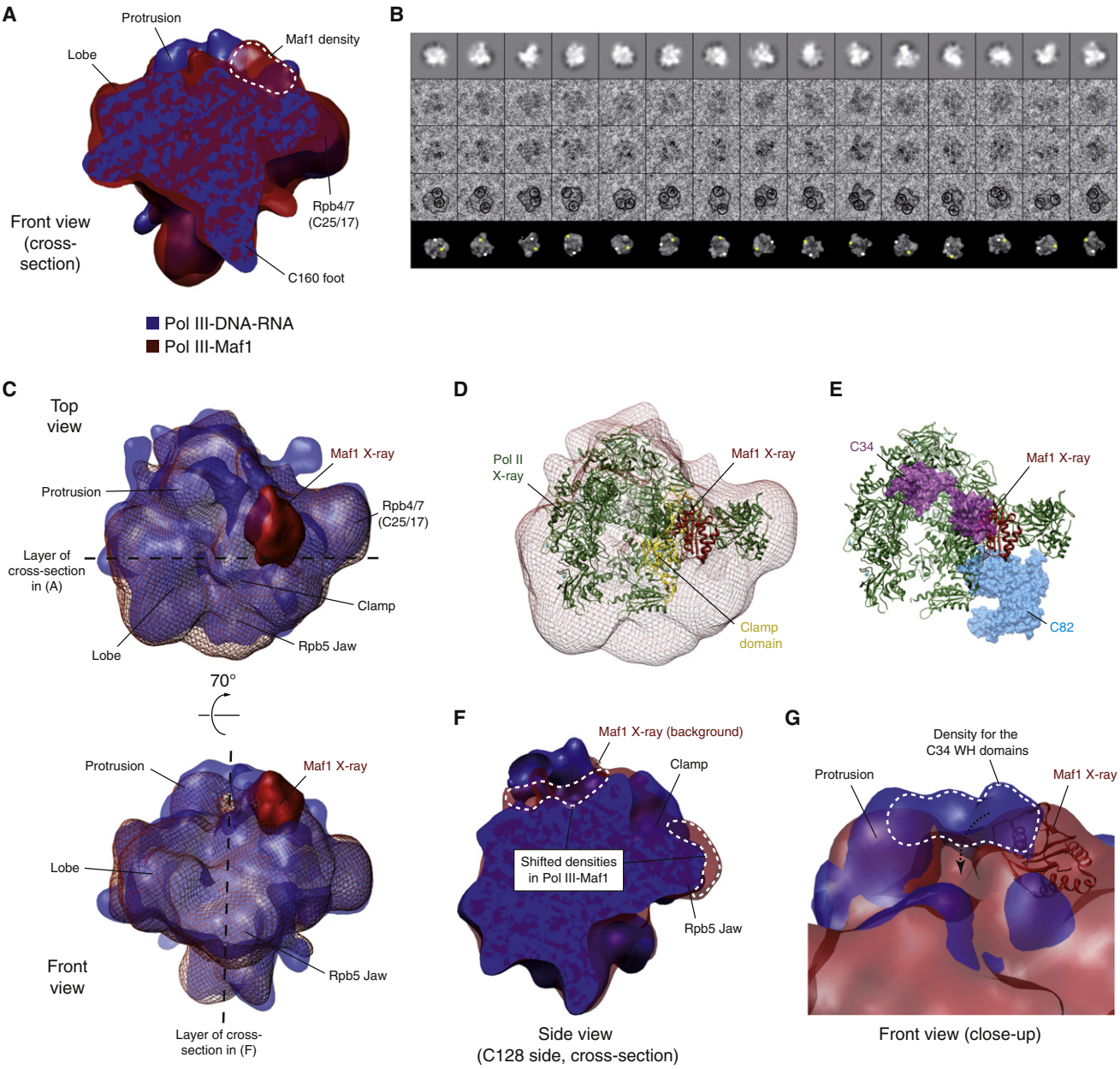

Figure 4. Cryo-EM Structure of the Pol III-Maf1 Complex

(A) Comparison of cross-section of EM structures of the Pol III-Maf1 complex (red) and the Pol III-DNA-RNA complex (blue) reveals an additional density for Maf1.

(B) Different views of reference projections of the Pol III-Maf1 3D reconstruction (top row), corresponding Nanogold-labeled particles used for alignment (second row), raw Nanogold-labeled particles (third row), Nanogold locations (circles) on the Pol III-Maf1 structure (forth row), and surface representations of reconstructions with the C128 N terminus and the location of Maf1 indicated by white and yellow dots, respectively (bottom row).

(C) Fit of the Maf1 X-ray structure (red surface, low-pass filtered to the resolution of the EM map) to the Pol III-Maf1 EM map (red grid). For comparison, the cryo-EM map of the Pol III-DNA-RNA complex is shown (blue).

(D) Ribbon representation of the Pol III-Maf1 complex. The Pol II X-ray structure (Armache et al., 2005) is shown in green, and the Maf1 structure in red. The clamp C160 residues 1–245 are yellow. The Pol III-Maf1 cryo-EM map is shown as a red mesh.

(E) Steric clash of Maf1 (red ribbon) with C34 (purple) and C82 (cyan) as observed in the Pol III-DNA-RNA complex.

(F) Comparison of cross-sections of EM structures of the Pol III-Maf1 complex (red) and the Pol III-DNA-RNA complex (blue) reveals a shift of the C82/34/31 subcomplex upon Maf1 binding.

(G) Close-up view of the region above the clamp. Parts of the C34 densities in the Pol III-DNA-RNA complex (blue) are absent in the Pol III-Maf1 complex (red).

See also Figures S3and S4 and Movie S1.

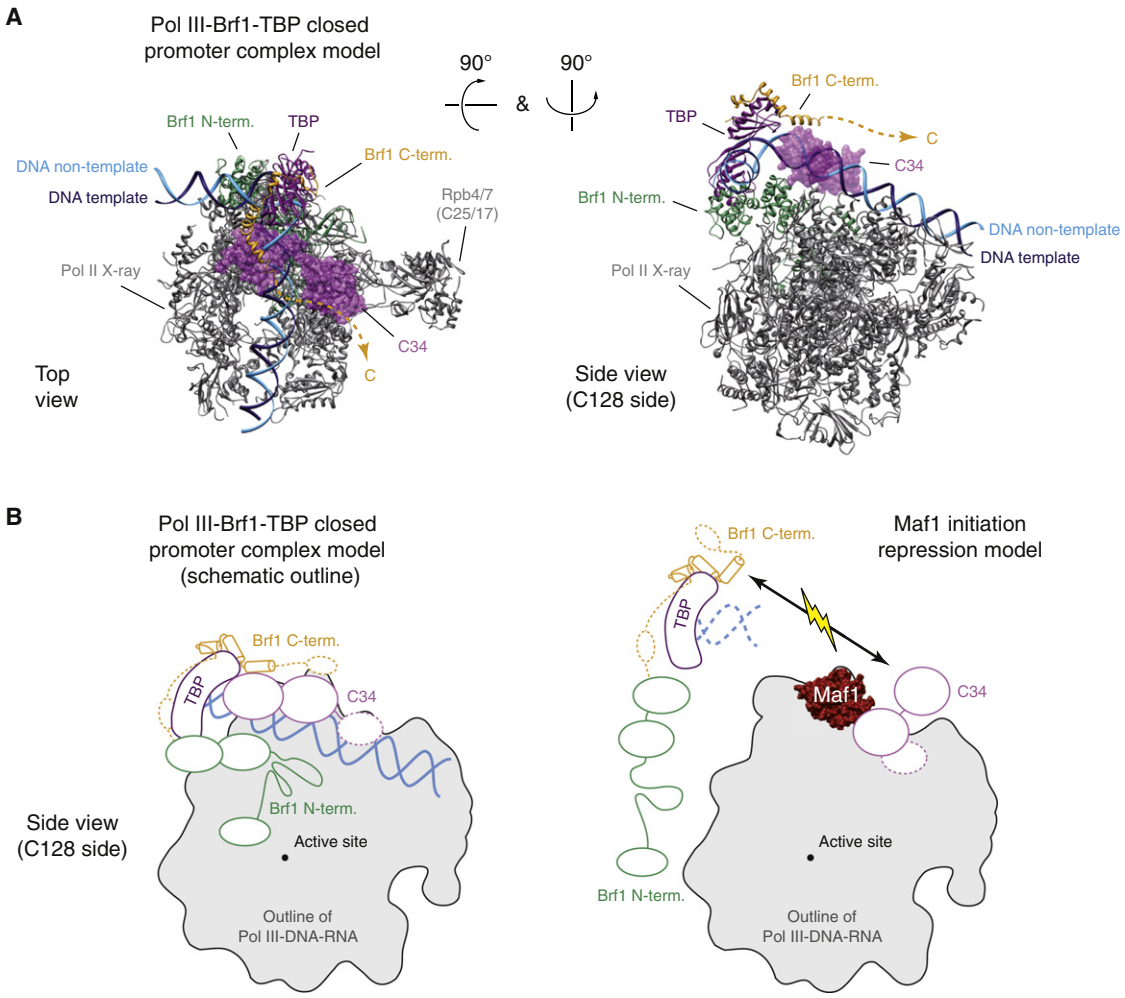

Figure 5. Mechanism of Pol III Repression by Maf1

(A) Model of the Pol III-Brf1-TBP-DNA closed promoter complex. The Pol II structure is silver, the C34 WH domains are magenta, the Brf1 N-terminal domain is green, the Brf1 C-terminal domain is orange, TBP is dark purple, and the closed promoter DNA is cyan/blue. The model is based on the homologous Pol II-TFIIB-TBP-DNA closed promoter complex model (Kostrewa et al., 2009) and the Brf1-TBP-DNA structure (Juo et al., 2003).

(B) Schematic view of Maf1-dependent repression of the formation of a Pol III-Brf1-TBP-DNA closed promoter complex. Colors are as in (A).

See also Figure S5.

1 mM PMSF, 1 mM benzamidine, 200 mM pepstatin, 60 mM leupeptin). The sample was applied to a 250 ml Biorex resin column (Biorad). Bound proteins were eluted with buffer C (buffer B + 500 mM KCl + 5 mM imidazole [pH 8.0]). The eluting proteins were loaded onto a 12 ml Ni-NTA Agarose (QIAGEN) column. Subsequent washing steps were performed with buffer C containing 10 mM imidazole and buffer D [40 mM HEPES (pH 7.8), 5 mM $MgCl_2$, 250 mM $(NH_4)_2SO_4$, 10% glycerol, 10 mM imidazole, 10 mM β-mercaptoethanol, 1 mM PMSF, 1 mM benzamidine, 200 mM pepstatin, 60 mM leupeptin]. Proteins were eluted with buffer D containing 250 mM imidazole and loaded onto a HiTrap Heparin 5 ml column (GE Healthcare) and fractionated by application of a salt gradient from 250 to 1000 mM $(NH_4)_2SO_4$ with buffer E (40 mM HEPES [pH 7.8], 5 mM $MgCl_2$, 20% glycerol, 0.5 mM EDTA, 10 mM β-mercaptoethanol, 1 mM PMSF, 1 mM benzamidine, 200 mM pepstatin, 60 mM leupeptin). Pooled fractions eluting at 500 mM $(NH_4)_2SO_4$ were diluted 5-fold with buffer E, loaded onto an anion exchange column (Mono Q 10/100 GL, GE Healthcare), and fractionated with a salt gradient from 50 to 1000 mM $(NH_4)_2SO_4$ in buffer F (40 mM HEPES [pH 7.8], 1 mM $MgCl_2$, 5 mM DTT). Pol III-containing fractions eluted at 600 mM $(NH_4)_2SO_4$, were pooled, diluted to a concentration of 50 mM $(NH_4)_2SO_4$, supplemented with a 10-fold molar excess of recombinant full-length C53/37 heterodimer, and incubated for 60 min. The sample was concentrated to 1 ml with an Amicon Ultra-4 centrifugal filter unit (MWCO 10 kDA, Millipore) and applied to gel filtration chromatography on a Superose 6 column (Superose 6 10/300 GL, GE Healthcare) with buffer G [20 mM HEPES pH 7.8, 50 mM $(NH_4)_2SO_4$, 100 μM $MgCl_2$, 10 μM $ZnCl_2$, 5 mM DTT]. Pol III-containing fractions were pooled, concentrated to 1 mg/ml with an Amicon Ultra-4 centrifugal filter unit (MWCO 10 kDA, Millipore) and flash frozen in liquid N_2 after addition of 10% glycerol.

Cryo-EM Structure Determinations

Purified Pol III was diluted to 0.1 mg/ml in buffer G and applied to glow-discharged precoated carbon holey grids (Quantifoil R3/3, 2 nm carbon on top). Samples were flash frozen in liquid ethane with a semiautomated controlled-environment system (Vitrobot, FEI Company) at 4°C, 95% humidity, and stored in liquid nitrogen until transfer to the microscope. Micrographs were recorded under low dose conditions of ~15 e/Å^2 on a FEI Tecnai Spirit microscope operating at 120 kV, equipped with a LaB_6 filament and a Gatan side entry

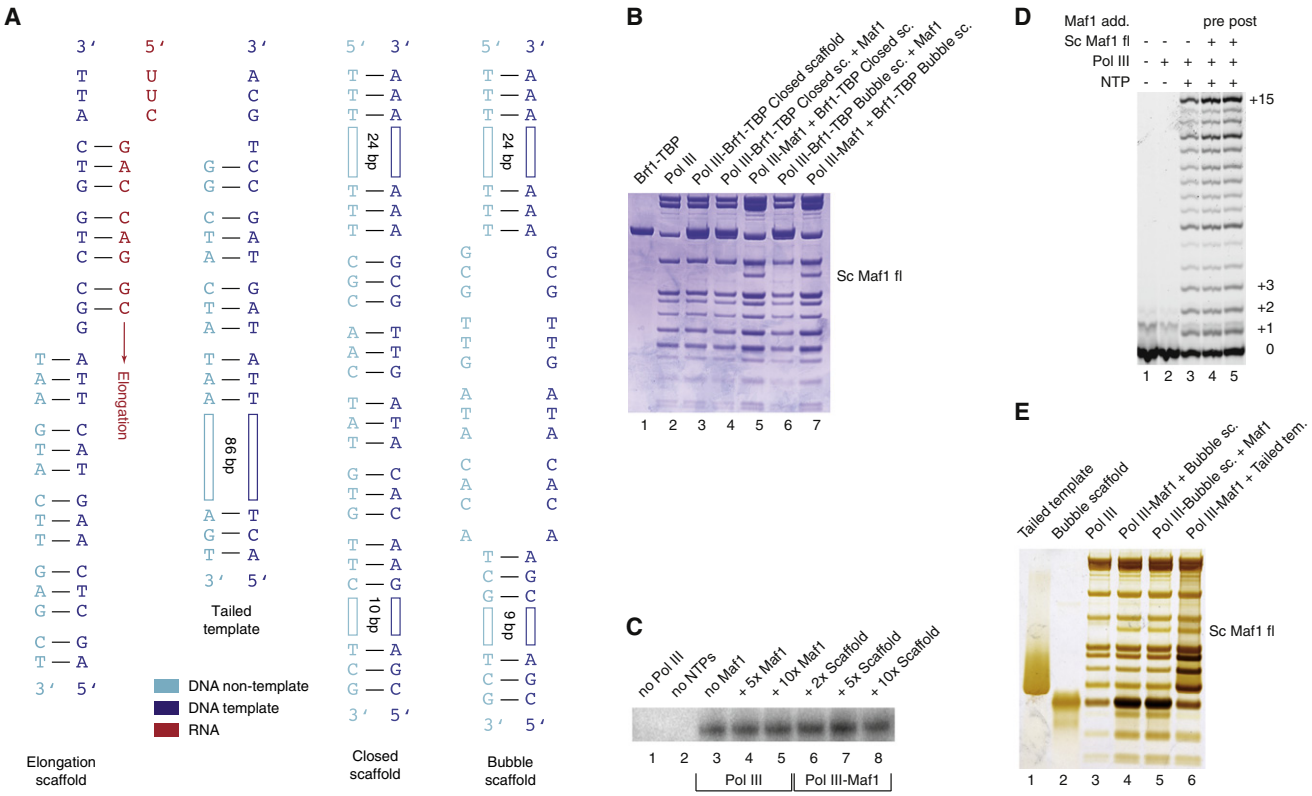

Figure 6. Maf1 Impairs Closed Promoter Complex Formation but Not Pol III Activity

(A) Nucleic acid scaffolds.

(B) Competition assays reveal that Maf1 impairs binding of Pol III to a Brf1-TBP-DNA complex. Preassembled Pol III-Brf1-TBP-DNA or Pol III-Maf1 complexes were incubated with a 5-fold molar excess of competing factor or complex as indicated and subjected to gel filtration, and the peak fraction was analyzed by SDS-PAGE. In lanes 3, 4, and 6, the presence of DNA was revealed by the high A_{260}/A_{280} ratio (~1) compared to the $A_{260}/_{280}$ ratio (~0.6) in lanes 2, 5, and 7.

(C) Factor-independent Pol III transcription assays. Preincubated Pol III-DNA (lanes 3–5) and Pol III-Maf1 complexes (lanes 6–8) efficiently transcribe the tailed template (A). Addition of increasing amounts of Maf1 to preincubated Pol III-DNA complexes does not impair transcription (lanes 4 and 5). Increased amounts of scaffold have no effect (lanes 6–8).

(D) RNA extension assay. The elongation scaffold (A) was efficiently transcribed to produce run-off product (+15) by Pol III upon addition of NTPs (lane 3). Preincubation or addition of Maf1 (lanes 4 or 5, respectively) did not impair activity.

(E) Pol III can simultaneously bind Maf1 and nucleic acids. Preassembled Pol III-Maf1 and Pol III-DNA complexes were incubated with 5-fold molar excess of DNA or Maf1, respectively, and subjected to gel filtration, and the peak fraction was analyzed by SDS-PAGE and silver staining. Staining of a Pol III-Maf1 complex (without DNA) is identical to that in lanes 4, 5, and 6.

cryoholder. Images were acquired at underfocus values in the range of 1.5–4 μm on a 2k × 2k FEI Eagle CCD camera applying a pre-exposure of 100 ms at a magnification of 90,000×, resulting in a pixel size of 3.31 Å/px on the object scale. Image-processing operations were carried out with SPIDER (Frank et al., 1996). Initial particle selection was performed with EMAN (Ludtke et al., 1999). Reference particles were picked manually to avoid discrepancies due to defocus and ice differences. Automatically selected particles were verified visually. Windowed particles were aligned to 83 projections of the Pol II X-ray structure (1Y1W, Gaussian low-pass filtered to 35 Å), which lacked the mobile OB and HRDC domains of Rpb4/7. Particle assignment to the reference projections was evenly distributed, barring few overrepresented outliers that were limited to prevent predominant views (Figure S1). Backprojection of the particle images with the angles from reference-based alignment resulted in a reconstruction that showed additional densities at the clamp and C25/17 and was used as a reference for 20 rounds of angular refinement. Images were backprojected in real space with the refined angles. The resulting reconstruction was Gaussian low-pass filtered to 25 Å and used as reference for another round of alignment and refinement, and this procedure was iterated until convergence. A 21 Å reconstruction of Pol III from a data set of 20,480 particles was obtained. During early stage of refinement, density for a complete C25/17 complex and other additional densities appeared that could be confirmed by an independent 23 Å reconstruction from 12,174 particles (data not shown). Projections of the 20,480 particle Pol III reconstruction, as well as their corresponding particle averages, were compared to averages resulting from a reference-free 2D alignment method with the program refine2d (Ludtke et al., 1999). A high portion of similar averages showed that the alignment and refinement based on the reference structure was not significantly biased. A cryo-EM data set of Pol III, prepared as above, incubated with a 3-fold molar excess of DNA-RNA scaffold, was collected, and a reconstruction at 19 Å resolution was obtained with 11,965 particles. A 18.5 Å reconstruction of a size-exclusion purified Pol III-Maf1 complex (see preparation for interaction assays) was obtained from 16,974 particles. The resolution of the structures could not be improved when 96,944 particles collected on film at 200 keV with a FEI Polara microscope were used.

Maf1 Crystal Structure Determination

DNA encoding *S. cerevisiae* or human Maf1 was PCR-amplified from genomic DNA and cloned into pET-28b vector (Novagen) with the NdeI/NotI restriction sites, resulting in a N-terminal hexahistidine tag. *E. coli* BL21 (DE3) RIL cells

(Stratagene) were transformed with the plasmid and grown in LB medium at 37°C to an OD_{600} of 0.6. Expression was induced with 0.5 mM IPTG for 16 hr at 18°C. Cells were lysed by sonification in buffer H (50 mM HEPES [pH 7.8], 0.5 M NaCl, 10 mM imidazole, 5 mM $MgCl_2$, 10 μM EDTA, 10% glycerol, 10 mM β-mercaptoethanol). After centrifugation, the supernatant was loaded onto a 3 ml Ni-NTA column (QIAGEN) equilibrated with buffer H, but 20 mM imidazole. The column was washed with 20 column volumes (CVs) and eluted with buffer H, but 300 mM imidazole. Proteins were purified by anion exchange chromatography (Mono Q, GE Healthcare). The column was equilibrated with buffer I (50 mM HEPES [pH 7.8], 5 mM MgCl2, 100 μM EDTA, 10 mM β-mercaptoethanol, 10% glycerol), and proteins were eluted with a linear gradient of 20 CVs from 10 mM to 1 M NaCl. After concentration, the sample was applied to a Superdex-75 size-exclusion column (GE Healthcare) equilibrated with buffer L (25 mM HEPES [pH 7.0], 25 mM NaCl, 5 mM DTT) for crystallization experiments or buffer M [50 mM HEPES (pH 7.8), 40 mM $(NH_4)_2SO_4$, 100 μM $MgCl_2$, 10 μM $ZnCl_2$, 5 mM DTT] for binding experiments. For partial proteolysis, 100 μl purified Maf1 at 1 mg/ml were mixed with 1 μg trypsin or chymotrypsin. The reactions were carried out at 37°C in buffer R containing 1 mM $CaCl_2$. Aliquots of 10 μl were taken at 1, 3, 5, 10, 30, and 60 min, and the reaction was stopped by addition of 5 × SDS sample buffer and incubation at 95°C for 5 min. Samples were analyzed by SDS-PAGE. The N termini of digestion products were analyzed by Edman sequencing. For crystallization, human Maf1 variant 1–35;83–205 was concentrated to 40 mg/ml. Crystals were grown within 2 days at 20°C in hanging drops over a reservoir solution containing 50 mM MES (pH 6.0) and 175 mM sodium oxalate. Native crystals were transferred into reservoir solution containing 25% glycerol and were flash cooled in liquid nitrogen. Crystals were soaked for 0.5–2 min in a reservoir solution containing 25% glycerol and 0.5 M NaBr and flash frozen in liquid nitrogen. Diffraction data were collected at 100 K on a PILATUS 6M detector at the Swiss Light Source (SLS), Villigen, Switzerland (Table 1). Three-wavelength anomalous diffraction data were collected from a bromide-soaked crystal. Data were processed with MOSFLM (Leslie et al., 1986) and scaled with SCALA (Evans, 2007), and data quality was assessed with Phenix.Xtriage (Adams et al., 2010). Program Phenix.HySS (Adams et al., 2010) identified six bromide sites that were used for phasing with program SOLVE (Terwilliger and Berendzen, 1999). Density modification was carried out with RESOLVE (Terwilliger, 2003). The model was built with COOT (Emsley and Cowtan, 2004) and refined with Phenix.Refine (Adams et al., 2010) to a free R factor of 21% (Table 1).

Nanogold Labeling

Size exclusion-purified Pol III was incubated for 60 min at 4°C in buffer N (buffer M + 15 mM imidazole) with a 10-fold molar excess of recombinant full-length Maf1. The complex was then incubated with a 20-fold molar excess of Ni-NTA-Nanogold (Nanoprobes, INC) for 30 min. The sample was concentrated to 1 ml with an Amicon Ultra-4 centrifugal filter unit (MWCO 10 kDa, Millipore) and applied to gel-filtration chromatography on a Superose 6 column (Superose 6 10/300 GL, GE Healthcare) with buffer G. Fractions were pooled and samples prepared for cryo-EM as above. Cryo-EM data were collected as for free Pol III but at an underfocus range of 3–4 μm to obtain high image contrast. A large portion of particles showed both His tags bound with Nanogold clusters. These were picked from the micrographs and aligned to projections of the Pol III-Maf1 reconstruction. The strong signal of the Nanogold was dampened in the images by manually applying a threshold to the histograms. The in-plane rotation parameters resulting from the alignment were applied to the original images, and the rotated images were compared to corresponding 2D surface views with the location of Maf1 and the N terminus of C128 indicated (Figure 4). The length of the His_6-tag and the ~0.9 nm linker between the gold cluster and the nickel-NTA group of the Nanogold reagent give an expected mean variability of ~2 nm radius that was taken into account. The gold signal on the N terminus of C128 displayed more apparent variability, which is explained by the presence of four additional tandem FLAG sequences.

Interaction and Transcription Assays

Brf1-TBP complex was obtained as a triple fusion protein as described (Kassavetis et al., 2005). Pol III-Brf1-TBP-DNA and Pol III-Maf1 complexes were preassembled with 5-fold molar excesses of Brf1-TBP-DNA and Maf1, respectively, in buffer M for 60 min at 4°C and purified by gel filtration (Superose 6 10/300 GL, GE Healthcare) in buffer M. Purified complexes were then incubated with a 5-fold molar excess of the competing factors, incubated in buffer M for 60 min at 4°C, applied again to gel filtration, and analyzed by SDS-PAGE. For the nucleic acid binding assay, size exclusion-purified complexes were analyzed by silver-stained gels. For factor-independent transcription assays, 1.5 pmol Pol III or Pol III-Maf1 complex were incubated for 30 min at 20°C with 2 pmol or variable amounts of a pre-annealed tailed-template scaffold (nontemplate DNA: 5′-GGCTACTATAAATAAATGTTTTTTTCGCAACTATGTGT TCGCGAAGTAACCCTTCGTGGACATTTGGTCAATTTGAAACAATACAGAGA TGATCAGCAGT-3′; template DNA: 5′-ACTGCTGATCATCTCTGTATTGTTTC AAATTGACCAAATGTCCACGAAGGGTTACTTCGCGAACACATAGTTGCGAA AAAAACATTTATTTATAGTAGCCTGCA-3′) in the presence of 0.5 mM GpG RNA primer. Complexes were incubated for 30 min at 20°C in the presence of 0.3 mM ATP, GTP, CTP, NS [α-^{32}P]UTP in 20 μl reaction mixtures containing 40 mM Tris-HCl (pH 8.0), 60 mM NaCl, 7 mM $MgCl_2$, 7% glycerol, 5 mM DTT. Reactions were stopped by addition of an equal volume of 2× loading buffer (8 M urea, 2× TBE) and incubation for 5 min at 95°C. RNA products were separated by denaturing gel electrophoresis and visualized with a Typhoon 9400 phosphoimager (GE Healthcare). For RNA extension assays, 5 pmol of Pol III or Pol III preincubated (10 min at 20°C) with a 5-fold molar excess of Maf1 was incubated for 30 min at 20°C with 5 pmol of a preannealed minimal nucleic acid scaffold (template DNA: 3′-TTACTGGTCCGGATTCATGAACTCGA-5′; nontemplate DNA: 5′-TAAGTACTTGAG-3′; RNA: 5′-FAM-UGCAUUUCGAC CAGGC-3′). Maf1 was added at a 5-fold molar excess, followed by incubation for 5 min at 20°C. For RNA elongation, complexes were incubated for 10 min with 1 mM NTPs at 28°C in transcription buffer (60 mM ammonium sulfate, 20 mM HEPES [pH 7.6], 8 mM magnesium sulfate, 10 μM zinc chloride, 10% glycerol, 10 mM DTT). Reactions were stopped and RNA products were separated and visualized as above.

ACCESSION NUMBERS

The coordinate file and structure factors for the Maf1 crystal structure were deposited in the Protein Data BBank under accession code 3NR5. The EM structures of Pol III, the Pol III-DNA-RNA complex, and the Pol III-Maf1 complex have been deposited in the EMDB database under accession codes EMD-1753, EMD-1754, and EMD-1755, respectively.

SUPPLEMENTAL INFORMATION

Supplemental Information includes five figures and one movie and can be found with this article online at doi:10.1016/j.cell.2010.09.002.

ACKNOWLEDGMENTS

We thank R. Beckmann, T. Becker, C. Ungewickel, J. Bürger, and T. Mielke for help with E.M. We thank A. Imhof (Zentrallabor für Proteinanalytik) and T. Fröhlich (Laboratory for Functional Genome Analysis) for mass spectrometry. We acknowledge the crystallization facility at the department of E. Conti at the Max Planck Institute of Biochemistry, Martinsried. We thank D. Deak for help with figure preparation. A.V. was supported by a European Molecular Biology Organization long-term fellowship and by the European Union training program Marie Curie (MEIF-CT-2006-040653). P.C. was supported by the Deutsche Forschungsgemeinschaft, the SFB646, the TR5, the Nanosystems Initiative Munich, the Elitenetzwerk Bayern, and the Jung-Stiftung. A.V. prepared Pol III complexes, A.V. and A.G.K. determined EM structures, R.R. prepared and crystallized Maf1, R.R. and A.V. determined the Maf1 X-ray structure, R.R. and A.V. conducted functional assays, G.A.K. advised on Pol III preparation, A.V., R.R., A.G.K., and P.C. wrote the manuscript, and P.C. designed and supervised research.

Received: May 3, 2010
Revised: July 6, 2010
Accepted: August 11, 2010
Published: September 30, 2010

REFERENCES

Adams, P.D., Afonine, P.V., Bunkóczi, G., Chen, V.B., Davis, I.W., Echols, N., Headd, J.J., Hung, L.W., Kapral, G.J., Grosse-Kunstleve, R.W., et al. (2010). PHENIX: a comprehensive Python-based system for macromolecular structure solution. Acta Crystallogr. D Biol. Crystallogr. *66*, 213–221.

Andrau, J.C., Sentenac, A., and Werner, M. (1999). Mutagenesis of yeast TFIIIB70 reveals C-terminal residues critical for interaction with TBP and C34. J. Mol. Biol. *288*, 511–520.

Armache, K.J., Mitterweger, S., Meinhart, A., and Cramer, P. (2005). Structures of complete RNA polymerase II and its subcomplex, Rpb4/7. J. Biol. Chem. *280*, 7131–7134.

Bardeleben, C., Kassavetis, G.A., and Geiduschek, E.P. (1994). Encounters of Saccharomyces cerevisiae RNA polymerase III with its transcription factors during RNA chain elongation. J. Mol. Biol. *235*, 1193–1205.

Bartholomew, B., Durkovich, D., Kassavetis, G.A., and Geiduschek, E.P. (1993). Orientation and topography of RNA polymerase III in transcription complexes. Mol. Cell. Biol. *13*, 942–952.

Boguta, M., Czerska, K., and Zoładek, T. (1997). Mutation in a new gene MAF1 affects tRNA suppressor efficiency in Saccharomyces cerevisiae. Gene *185*, 291–296.

Brueckner, F., Hennecke, U., Carell, T., and Cramer, P. (2007). CPD damage recognition by transcribing RNA polymerase II. Science *315*, 859–862.

Brun, I., Sentenac, A., and Werner, M. (1997). Dual role of the C34 subunit of RNA polymerase III in transcription initiation. EMBO J. *16*, 5730–5741.

Cabart, P., Lee, J., and Willis, I.M. (2008). Facilitated recycling protects human RNA polymerase III from repression by Maf1 in vitro. J. Biol. Chem. *283*, 36108–36117.

Carter, R., and Drouin, G. (2009). The evolutionary rates of eukaryotic RNA polymerases and of their transcription factors are affected by the level of concerted evolution of the genes they transcribe. Mol. Biol. Evol. *26*, 2515–2520.

Chédin, S., Riva, M., Schultz, P., Sentenac, A., and Carles, C. (1998). The RNA cleavage activity of RNA polymerase III is mediated by an essential TFIIS-like subunit and is important for transcription termination. Genes Dev. *12*, 3857–3871.

Chen, Z.A., Jawhari, A., Fischer, L., Buchen, C., Tahir, S., Kamenski, T., Rasmussen, M., Lariviere, L., Bukowski-Wills, J.C., Nilges, M., et al. (2010). Architecture of the RNA polymerase II-TFIIF complex revealed by cross-linking and mass spectrometry. EMBO J. *29*, 717–726.

Cramer, P., Armache, K.J., Baumli, S., Benkert, S., Brueckner, F., Buchen, C., Damsma, G.E., Dengl, S., Geiger, S.R., Jasiak, A.J., et al. (2008). Structure of eukaryotic RNA polymerases. Annu. Rev. Biophys. *37*, 337–352.

Damsma, G.E., and Cramer, P. (2009). Molecular basis of transcriptional mutagenesis at 8-oxoguanine. J. Biol. Chem. *284*, 31658–31663.

Dephoure, N., Zhou, C., Villén, J., Beausoleil, S.A., Bakalarski, C.E., Elledge, S.J., and Gygi, S.P. (2008). A quantitative atlas of mitotic phosphorylation. Proc. Natl. Acad. Sci. USA *105*, 10762–10767.

Desai, N., Lee, J., Upadhya, R., Chu, Y., Moir, R.D., and Willis, I.M. (2005). Two steps in Maf1-dependent repression of transcription by RNA polymerase III. J. Biol. Chem. *280*, 6455–6462.

Eichner, J., Chen, H.T., Warfield, L., and Hahn, S. (2010). Position of the general transcription factor TFIIF within the RNA polymerase II transcription preinitiation complex. EMBO J. *29*, 706–716.

Emsley, P., and Cowtan, K. (2004). Coot: model-building tools for molecular graphics. Acta Crystallogr. D Biol. Crystallogr. *60*, 2126–2132.

Evans, P. (2007). SCALA - Scale Together Multiple Observations of Reflections. (Cambridge: MRC Laboratory of Molecular Biology).

Fernández-Tornero, C., Böttcher, B., Riva, M., Carles, C., Steuerwald, U., Ruigrok, R.W., Sentenac, A., Müller, C.W., and Schoehn, G. (2007). Insights into transcription initiation and termination from the electron microscopy structure of yeast RNA polymerase III. Mol. Cell *25*, 813–823.

Ferri, M.L., Peyroche, G., Siaut, M., Lefebvre, O., Carles, C., Conesa, C., and Sentenac, A. (2000). A novel subunit of yeast RNA polymerase III interacts with the TFIIB-related domain of TFIIIB70. Mol. Cell. Biol. *20*, 488–495.

Frank, J., Radermacher, M., Penczek, P., Zhu, J., Li, Y., Ladjadj, M., and Leith, A. (1996). SPIDER and WEB: processing and visualization of images in 3D electron microscopy and related fields. J. Struct. Biol. *116*, 190–199.

Gavin, A.C., Aloy, P., Grandi, P., Krause, R., Boesche, M., Marzioch, M., Rau, C., Jensen, L.J., Bastuck, S., Dümpelfeld, B., et al. (2006). Proteome survey reveals modularity of the yeast cell machinery. Nature *440*, 631–636.

Geiduschek, E.P., and Kassavetis, G.A. (2001). The RNA polymerase III transcription apparatus. J. Mol. Biol. *310*, 1–26.

Geiduschek, E.P., and Kassavetis, G.A. (2006). Transcription: adjusting to adversity by regulating RNA polymerase. Curr. Biol. *16*, R849–R851.

Geiger, S.R., Lorenzen, K., Schreieck, A., Hanecker, P., Kostrewa, D., Heck, A.J.R., and Cramer, P. (2010). RNA polymerase I contains a TFIIF-related DNA-binding subcomplex. Mol. Cell *39*, 583–594.

Grummt, I. (2003). Life on a planet of its own: regulation of RNA polymerase I transcription in the nucleolus. Genes Dev. *17*, 1691–1702.

Holm, L., and Park, J. (2000). DaliLite workbench for protein structure comparison. Bioinformatics *16*, 566–567.

Jasiak, A.J., Armache, K.J., Martens, B., Jansen, R.P., and Cramer, P. (2006). Structural biology of RNA polymerase III: subcomplex C17/25 X-ray structure and 11 subunit enzyme model. Mol. Cell *23*, 71–81.

Juo, Z.S., Kassavetis, G.A., Wang, J., Geiduschek, E.P., and Sigler, P.B. (2003). Crystal structure of a transcription factor IIIB core interface ternary complex. Nature *422*, 534–539.

Kassavetis, G.A., Han, S., Naji, S., and Geiduschek, E.P. (2003). The role of transcription initiation factor IIIB subunits in promoter opening probed by photochemical cross-linking. J. Biol. Chem. *278*, 17912–17917.

Kassavetis, G.A., Soragni, E., Driscoll, R., and Geiduschek, E.P. (2005). Reconfiguring the connectivity of a multiprotein complex: fusions of yeast TATA-binding protein with Brf1, and the function of transcription factor IIIB. Proc. Natl. Acad. Sci. USA *102*, 15406–15411.

Kassavetis, G.A., Prakash, P., and Shim, E. (2010). The C53/C37 subcomplex of RNA polymerase III lies near the active site and participates in promoter opening. J. Biol. Chem. *285*, 2695–2706.

Khoo, B., Brophy, B., and Jackson, S.P. (1994). Conserved functional domains of the RNA polymerase III general transcription factor BRF. Genes Dev. *8*, 2879–2890.

Kostrewa, D., Zeller, M.E., Armache, K.J., Seizl, M., Leike, K., Thomm, M., and Cramer, P. (2009). RNA polymerase II-TFIIB structure and mechanism of transcription initiation. Nature *462*, 323–330.

Krissinel, E., and Henrick, K. (2004). Secondary-structure matching (SSM), a new tool for fast protein structure alignment in three dimensions. Acta Crystallogr. D Biol. Crystallogr. *60*, 2256–2268.

Landrieux, E., Alic, N., Ducrot, C., Acker, J., Riva, M., and Carles, C. (2006). A subcomplex of RNA polymerase III subunits involved in transcription termination and reinitiation. EMBO J. *25*, 118–128.

Lannutti, B.J., Persinger, J., and Bartholomew, B. (1996). Probing the protein-DNA contacts of a yeast RNA polymerase III transcription complex in a crude extract: solid phase synthesis of DNA photoaffinity probes containing a novel photoreactive deoxycytidine analog. Biochemistry *35*, 9821–9831.

Lee, J., Moir, R.D., and Willis, I.M. (2009). Regulation of RNA polymerase III transcription involves SCH9-dependent and SCH9-independent branches of the target of rapamycin (TOR) pathway. J. Biol. Chem. *284*, 12604–12608.

Leslie, A.G.W., Brick, P., and Wonacott, A.T. (1986). Daresbury Lab. Inf. Quart. Protein Crystallogr. *18*, 33–39.

Lorenzen, K., Vannini, A., Cramer, P., and Heck, A.J. (2007). Structural biology of RNA polymerase III: mass spectrometry elucidates subcomplex architecture. Structure *15*, 1237–1245.

Ludtke, S.J., Baldwin, P.R., and Chiu, W. (1999). EMAN: semiautomated software for high-resolution single-particle reconstructions. J. Struct. Biol. *128*, 82–97.

Moir, R.D., Lee, J., Haeusler, R.A., Desai, N., Engelke, D.R., and Willis, I.M. (2006). Protein kinase A regulates RNA polymerase III transcription through the nuclear localization of Maf1. Proc. Natl. Acad. Sci. USA *103*, 15044–15049.

Oficjalska-Pham, D., Harismendy, O., Smagowicz, W.J., Gonzalez de Peredo, A., Boguta, M., Sentenac, A., and Lefebvre, O. (2006). General repression of RNA polymerase III transcription is triggered by protein phosphatase type 2A-mediated dephosphorylation of Maf1. Mol. Cell *22*, 623–632.

Paule, M.R., and White, R.J. (2000). Survey and summary: transcription by RNA polymerases I and III. Nucleic Acids Res. *28*, 1283–1298.

Pluta, K., Lefebvre, O., Martin, N.C., Smagowicz, W.J., Stanford, D.R., Ellis, S.R., Hopper, A.K., Sentenac, A., and Boguta, M. (2001). Maf1p, a negative effector of RNA polymerase III in Saccharomyces cerevisiae. Mol. Cell. Biol. *21*, 5031–5040.

Reina, J.H., Azzouz, T.N., and Hernandez, N. (2006). Maf1, a new player in the regulation of human RNA polymerase III transcription. PLoS ONE *1*, e134.

Roberts, D.N., Wilson, B., Huff, J.T., Stewart, A.J., and Cairns, B.R. (2006). Dephosphorylation and genome-wide association of Maf1 with Pol III-transcribed genes during repression. Mol. Cell *22*, 633–644.

Sadhale, P.P., and Woychik, N.A. (1994). C25, an essential RNA polymerase III subunit related to the RNA polymerase II subunit RPB7. Mol. Cell. Biol. *14*, 6164–6170.

Schramm, L., and Hernandez, N. (2002). Recruitment of RNA polymerase III to its target promoters. Genes Dev. *16*, 2593–2620.

Shor, B., Wu, J., Shakey, Q., Toral-Barza, L., Shi, C., Follettie, M., and Yu, K. (2010). Requirement of the mTOR kinase for the regulation of Maf1 phosphorylation and control of RNA polymerase III-dependent transcription in cancer cells. J. Biol. Chem. *285*, 15380–15392.

Terwilliger, T.C. (2003). SOLVE and RESOLVE: automated structure solution and density modification. Methods Enzymol. *374*, 22–37.

Terwilliger, T.C., and Berendzen, J. (1999). Automated MAD and MIR structure solution. Acta Crystallogr. D Biol. Crystallogr. *55*, 849–861.

Thuillier, V., Stettler, S., Sentenac, A., Thuriaux, P., and Werner, M. (1995). A mutation in the C31 subunit of Saccharomyces cerevisiae RNA polymerase III affects transcription initiation. EMBO J. *14*, 351–359.

Upadhya, R., Lee, J., and Willis, I.M. (2002). Maf1 is an essential mediator of diverse signals that repress RNA polymerase III transcription. Mol. Cell *10*, 1489–1494.

Wang, Z., and Roeder, R.G. (1997). Three human RNA polymerase III-specific subunits form a subcomplex with a selective function in specific transcription initiation. Genes Dev. *11*, 1315–1326.

Warner, J.R. (1999). The economics of ribosome biosynthesis in yeast. Trends Biochem. Sci. *24*, 437–440.

Werner, M., Hermann-Le Denmat, S., Treich, I., Sentenac, A., and Thuriaux, P. (1992). Effect of mutations in a zinc-binding domain of yeast RNA polymerase C (III) on enzyme function and subunit association. Mol. Cell. Biol. *12*, 1087–1095.

Werner, M., Chaussivert, N., Willis, I.M., and Sentenac, A. (1993). Interaction between a complex of RNA polymerase III subunits and the 70-kDa component of transcription factor IIIB. J. Biol. Chem. *268*, 20721–20724.

Willis, I.M., Desai, N., and Upadhya, R. (2004). Signaling repression of transcription by RNA polymerase III in yeast. Prog. Nucleic Acid Res. Mol. Biol. *77*, 323–353.